The Astrophysical Journal, 660:1451–1461, 2007 May 10

THE LOWEST MASS WHITE DWARF

Mukremin Kilic,[1] Carlos Allende Prieto,[2] Warren R. Brown,[3] and D. Koester[4]

Received 2006 November 15; accepted 2007 February 11

ABSTRACT

Extremely low mass white dwarfs are very rare objects likely formed in compact binary systems. We present MMT optical spectroscopy of 42 low-mass white dwarf candidates serendipitously discovered in a survey for hypervelocity B-type stars. One of these objects, SDSS J0917+46, has $T_{\rm eff} = 11{,}288 \pm 72$ K and $\log g = 5.48 \pm 0.03$; with an estimated mass of 0.17 $M_\odot$, it is the lowest gravity/mass white dwarf currently known. However, 40 of the low-mass candidates are normal DA white dwarfs with apparently inaccurate SDSS g magnitudes. We revisit the identification of low-mass white dwarf candidates previously found in the SDSS and conclude that four objects have $M < 0.2$ $M_\odot$. None of these white dwarfs show excess emission from a binary companion, and radial velocity searches will be necessary to constrain the nature of the unseen companions.

Subject headings: stars: low-mass, brown dwarfs — white dwarfs

Online material: color figures

1. INTRODUCTION

The mass distribution of hot DA (hydrogen-rich atmosphere) white dwarfs (WDs) from the Palomar Green Survey peaks at 0.57 $M_\odot$ with a dispersion of 0.19 $M_\odot$ (Liebert et al. 2005). A similar mass distribution is also observed for WDs cooler than 12,000 K (Bergeron et al. 2001). In both cases, separate low-mass and high-mass components to this mass distribution are also observed. The Liebert et al. sample includes WDs with masses as low as 0.32 $M_\odot$, and the mass distribution has a low-mass peak at 0.40 $M_\odot$. These low-mass WDs are understood as He core WDs formed in binary systems. He core WDs can be formed when a companion strips the outer envelope from a post-main-sequence star before the star reaches the tip of the red giant branch and ignites the helium. Low-mass WDs are usually found in close binaries, mostly double degenerate systems (Marsh et al. 1995). The Galaxy is not old enough to produce these WDs through single-star evolution.

Recent discoveries of extremely low mass (ELM; $\log g < 7$) WDs in the field and around pulsars show that some of these WDs retain only a small fraction of their progenitor mass and end up with as little mass as 0.2 $M_\odot$. Liebert et al. (2004) were the first to discover an ELM WD in the field (SDSS J1234−02) with $T_{\rm eff} = 17{,}470 \pm 750$ K and $\log g = 6.38 \pm 0.05$. Eisenstein et al. (2006) increased the number of ELM WD candidates found in the Sloan Digital Sky Survey (SDSS) to 13, including two objects with $\log g < 6$. Kawka et al. (2006) added one more object to the list (LP 400-22) with $\log g = 6.32 \pm 0.08$. The optical photometry of none of these objects shows an excess, and the nature of the companions to these objects is not known.

The existence of ELM WDs around pulsars suggests that neutron star companions may be responsible for creating such low-mass WDs. PSR J0437−4715, J0751+1807, J1012+5307, J1713+0747, B1855+09, and J1909−3744 are pulsars in circular pulsar-He WD binary systems with orbital periods of ~0.2–100 days (Nice et al. 2005). The properties of the pulsars in these systems differ markedly from those of typical isolated pulsars, showing more rapid spin periods and smaller inferred magnetic fields. They also tend to have masses greater than the canonical value of 1.35 $M_\odot$. The relatively high masses of pulsars in these systems presumably result from extended mass accretion during the late stages of their evolution (Nice et al. 2005). At the cessation of mass transfer, the neutron star turns on as a millisecond radio pulsar and the companion is left as a helium core WD (van Kerkwijk et al. 2000).

Optical spectroscopy of two of the low-mass WD companions to pulsars are available in the literature; van Kerkwijk et al. (1996) found a best-fit solution of $T_{\rm eff} = 8550 \pm 25$ K and $\log g = 6.75 \pm 0.07$ for the companion to PSR J1012+5307, whereas Bassa et al. (2006) measured $T_{\rm eff} = 10{,}090 \pm 150$ K and $\log g = 6.44 \pm 0.20$ for the companion to PSR J1911−5958A. In addition, Heber et al. (2003) found a subluminous B (sdB) star, HD 188112, with $T_{\rm eff} = 21{,}500 \pm 500$ K and $\log g = 5.66 \pm 0.05$ and suggested that it is the progenitor of a helium core WD. HD 188112 is in a binary system with an $M > 0.73$ $M_\odot$ compact object, a WD or a neutron star.

Recently, Brown et al. (2006) performed a search for hypervelocity stars in the SDSS Fourth Data Release. They used the SDSS photometry to select faint B star candidates in a survey area of ~3000 deg^2. They obtained follow-up spectroscopy of 247 candidates with the Blue Channel Spectrograph on the 6.5 m MMT telescope, 44 of which turned out to be WDs. The SDSS colors for ELM WDs fall into the same region as their selection region for B-type stars; thus, they identify all of these WDs as potential low-mass WDs with $\log g < 7$. Figure 1 shows $u-g$ versus $g-r$ color-color diagram of the low-mass WD candidates from Brown et al. (2006; *circles*) and Eisenstein et al. (2006; *triangles*). Our synthetic photometry of WD model atmospheres with $\log g =$ 5, 6, 7, and 8 (Finley et al. 1997) are shown as solid lines. B-type stars found in Brown et al.'s survey are shown as crosses. It is clear from this figure that all of the WDs found by Brown et al. (2006) lie to the right of the $\log g = 7$ line and are candidate low-mass WDs. In addition, one of these WDs has colors similar to the lowest mass WD candidate identified by Eisenstein et al. (2006).

[1] Columbus Fellow, Department of Astronomy, Ohio State University, Columbus, OH 43210; kilic@astronomy.ohio-state.edu.

[2] McDonald Observatory and Department of Astronomy, University of Texas, Austin, TX 78712; callende@astro.as.utexas.edu.

[3] Smithsonian Astrophysical Observatory, Cambridge, MA 02138; wbrown@cfa.harvard.edu.

[4] Institut für Theoretische Physik und Astrophysik, University of Kiel, 24098 Kiel, Germany; koester@astrophysik.uni-kiel.de.

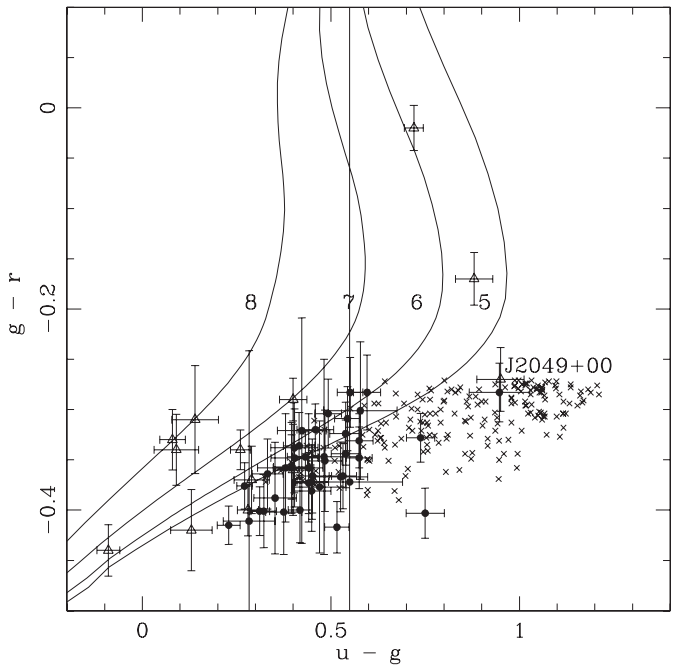

FIG. 1.—Color-color diagram for the low-mass WD candidates from Brown et al. (2006; *circles*) and Eisenstein et al. (2006; *triangles*). The lowest mass WD candidate found by Eisenstein et al. (2006), SDSS J2049+00, is labeled. Our synthetic photometry of WD model atmospheres with log $g = 8$, 7, 6, and 5 (Finley et al. 1997) are shown as solid lines. Late-B stars found in Brown et al.'s (2006) survey are shown as crosses. [*See the electronic edition of the Journal for a color version of this figure.*]

There are currently five confirmed ELM WDs (SDSS J1234−02, LP 400-22, HD 188112, and companions to PSR J1012+5307 and J1911−5958A) and 12 more SDSS candidates identified by Eisenstein et al. (2006). In this paper, we analyze the spectra of the low-mass WD candidates observed at the MMT by performing temperature and surface gravity fits to grids of pure hydrogen atmosphere models of Finley et al. (1997). We also revisit the model fits to the Eisenstein et al. (2006) low-mass WD sample. Our fitting procedures and the measured parameters for the MMT sample are discussed in § 2. Section 3 describes our efforts to understand the SDSS low-mass WD sample, and results from this analysis are discussed in § 4.

2. THE MMT SAMPLE

Brown et al. (2006) identified 44 WDs, including 42 DA WDs, a helium-rich (DB) WD, and another metal-rich (DZ) WD with Ca H and K lines. Here we exclude the two non-DA WDs from our analysis. The SDSS positions and dereddened photometry for our sample are given in Table 1. The g-band magnitudes for these WDs range from 17.3 to 20.1. The exposure times for the MMT spectroscopy were in the range 210–1800 s. Most spectra were obtained with a 1.25″ slit yielding a resolving power of $R = 3500$; however, several of them were obtained with a 1.0″ or 1.5″ slit that resulted in $R = 4300$ or 2900. All spectra were obtained at the parallactic angle. The spectra were flux calibrated using the blue spectrophotometric standards (Massey et al. 1988). Repeat observations of one of our WD candidates over four nights showed that the wavelength-dependent variations in the continuum shape are of order 6% for our typical WD spectra. Hence, the relative flux levels at different wavelengths are reliable at the 6% level.

2.1. *Spectroscopic Analysis*

The first step in our analysis is to smooth the observed spectra to a common resolving power in order to compare them with the same set of WD model atmospheres. We have chosen to smooth the spectra to $R = 2500$. This also increases slightly the signal-to-noise ratio (S/N) of the observed spectra. We use the radial velocities measured by Brown et al. (2006) to correct the spectra to the rest frame. After smoothing the spectra by convolution with a Gaussian kernel of the appropriate width, and resampling with 4 points per resolution element (constant step in log λ), the spectra were normalized using two different procedures: (1) determining the continuum by iteratively fitting a polynomial (six iterations), then dividing by the fit; and (2) dividing each spectrum by its median value. In the first case, the shape of the spectral energy distribution (SED) is effectively removed, losing valuable information but avoiding systematic errors in the flux calibration and the effects of reddening. We note that we apply the same procedures to both the observed and model spectra in all cases.

The grid of WD model atmospheres covers effective temperatures from 6000 to 30,000 K in steps of 1000 K, and surface gravities from log $g = 5.0$ to 9.0 in steps of 0.25 dex. The best-fit parameters are determined for each star by searching for the minimum χ^2 in the range covered by the spectrum using the Nelder-Mead algorithm (Nelder & Mead 1965), performing quadratic Bezier interpolation of the spectra in both $T_{\rm eff}$ and log g (Allende Prieto 2004). In the case of full continuum normalization (case 1), we only fit the Balmer line profiles, whereas we fit the entire spectrum in case 2. The derived error bars for the parameters are simply the square roots of the diagonal elements of the covariance matrix (Press et al. 1986).

If the analysis is carried out at different resolving powers, the results change slightly for case 1, where we fit the Balmer lines. We have repeated our fits with R changing from 2500 to 200, and found that the drift can be approximately matched with a $1/R$ law. We find that a reduction of resolving power from infinity to 2500 causes $T_{\rm eff}$ to be overestimated by 1% and log g by 0.04 dex. Since our spectra are mostly composed of strong Balmer lines, it is hard to determine the continuum in the blue part of the spectrum. In addition, the removal of the continuum sacrifices useful information and, in the presence of noise, introduces degeneracy—a decrease in $T_{\rm eff}$ can be compensated by an increase in log g, and multiple minima are apparent, although one is usually significantly deeper than the other.

In case 2, where we fit the entire spectrum, the parameters that we derive are independent of the resolution that we use down to $R > 200$; therefore, these results are more robust than those derived from the normalized spectra. In addition, the degeneracy problem is resolved with the additional information contained in the continuum shape. A comparison of our fits for cases 1 and 2 shows that on average our temperature and log g estimates differ by ∼800 K and 0.07 dex, respectively. Figure 2 shows the log g for our spectral fits using the line profiles from the continuum-corrected spectra (case 1) versus using the spectra without any continuum correction (case 2). This figure suggests that our gravity estimates are robust. With the exception of four objects for which flux calibration errors are apparent in the observed spectra (Cand 17, 20, 124, and 192),[5] the quality of our fits (minimum χ^2) is always better when the continuum shape is not removed.

We prefer the $T_{\rm eff}$ and log g from our best-fit case 2 solutions. Our fits to the original spectra contain more information than

[5] Cand 192 has an apparent Ca I line at 4226 Å. Ca II lines may be present in the spectrum, but not easily recognizable due to noisier spectrum in the blue. Our best-fit $T_{\rm eff} = 13{,}000$ K solution suggests that if the calcium was photospheric, we would expect to see strong Ca II lines in the spectrum of this object (see the optical spectrum of the metal-rich WD GD362 in Gianninas et al. 2004). The observed Ca I line may come from a late-type companion to this otherwise normal WD.

TABLE 1
Low-Mass White Dwarf Candidates Observed at the MMT

Name	SDSS J	g	$u-g$	$g-r$	$r-i$	$i-z$	$T_{\rm eff}$ (K)	log g	χ^2
Cand 17	145859.60+431113.3	19.201	0.539	−0.324	−0.228	−0.320	13000 ± 319	7.72 ± 0.04	1.95
Cand 20	151027.67+412520.1	19.008	0.484	−0.351	−0.262	−0.478	12420 ± 128	7.58 ± 0.02	2.53
Cand 25	152905.82+330520.4	18.288	0.575	−0.331	−0.185	−0.142	11519 ± 66	8.11 ± 0.02	1.18
Cand 36	155708.48+282336.0	17.496	0.532	−0.366	−0.223	−0.211	12044 ± 65	7.74 ± 0.02	1.13
Cand 102	002803.34−001213.4	18.346	0.516	−0.417	−0.263	−0.237	14788 ± 61	7.86 ± 0.02	1.36
Cand 106	010044.69−005034.1	19.981	0.578	−0.301	−0.113	−0.032	16248 ± 139	7.39 ± 0.05	1.35
Cand 107	010657.83−100839.3	19.287	0.526	−0.367	−0.168	−0.089	15263 ± 68	7.71 ± 0.02	1.36
Cand 108	011130.67+141049.8	19.818	0.380	−0.358	−0.236	−0.309	17426 ± 84	7.88 ± 0.02	1.34
Cand 116	020232.30−084918.3	19.117	0.482	−0.347	−0.125	−0.151	10678 ± 47	8.56 ± 0.02	1.20
Cand 124	031240.49−005941.1	19.367	0.283	−0.411	−0.417	−0.192	17251 ± 50	7.70 ± 0.01	1.63
Cand 128	074508.15+182630.0	19.295	0.750	−0.403	−0.195	−0.140	11000 ± 43	8.23 ± 0.01	1.27
Cand 133	075637.74+203730.7	18.578	0.229	−0.415	−0.297	−0.497	17177 ± 61	7.87 ± 0.02	1.44
Cand 137	080234.62+432301.1	18.356	0.432	−0.347	−0.264	−0.324	13458 ± 111	7.76 ± 0.01	1.40
Cand 144	082003.03+250012.1	19.454	0.449	−0.381	−0.093	−0.333	12844 ± 84	7.94 ± 0.01	1.28
Cand 150	083303.03+365906.3	17.930	0.947	−0.283	−0.283	−0.229	13399 ± 120	7.76 ± 0.02	1.31
Cand 164	085652.65+233341.8	18.389	0.311	−0.401	−0.163	−0.331	14255 ± 55	7.80 ± 0.01	1.22
Cand 171	091709.55+463821.8	18.696	0.738	−0.328	−0.237	−0.219	11288 ± 72	5.48 ± 0.03	1.45
Cand 176	092918.13+374529.9	19.325	0.470	−0.377	−0.287	−0.160	16480 ± 55	7.51 ± 0.02	1.07
Cand 186	095030.48+385713.2	18.347	0.322	−0.401	−0.314	−0.179	17788 ± 45	7.79 ± 0.01	1.02
Cand 192	095641.27+685727.5	18.056	0.550	−0.372	−0.364	−0.346	13000 ± 127	7.75 ± 0.02	5.18
Cand 193	095717.31+552839.2	18.678	0.352	−0.388	−0.337	−0.334	16381 ± 57	7.76 ± 0.02	1.28
Cand 203	100929.84+411205.2	19.424	0.404	−0.348	−0.233	−0.186	14621 ± 90	7.93 ± 0.02	1.22
Cand 205	101519.62+595430.5	17.920	0.544	−0.309	−0.181	−0.159	14965 ± 71	7.82 ± 0.03	1.05
Cand 207	101557.01+510428.4	18.707	0.575	−0.348	−0.191	−0.102	16316 ± 59	7.84 ± 0.02	1.36
Cand 208	101647.50+375835.2	17.279	0.375	−0.402	−0.303	−0.299	16908 ± 37	7.81 ± 0.01	1.17
Cand 225	104650.53+510028.6	17.867	0.418	−0.400	−0.269	−0.273	15866 ± 61	7.88 ± 0.02	1.29
Cand 352	073734.88+215017.3	19.208	0.459	−0.320	−0.088	−0.432	12138 ± 56	7.92 ± 0.01	1.10
Cand 362	082542.49+080100.5	19.342	0.451	−0.366	−0.313	−0.347	14087 ± 95	7.83 ± 0.02	1.13
Cand 363	082823.55+470001.4	17.634	0.423	−0.321	−0.188	−0.446	14526 ± 58	7.67 ± 0.02	1.40
Cand 369	084823.75+050845.2	17.027	0.271	−0.376	−0.256	−0.287	15332 ± 38	7.18 ± 0.01	1.21
Cand 371	085141.58+425117.7	18.267	0.493	−0.304	−0.248	−0.147	12337 ± 57	7.92 ± 0.01	1.15
Cand 375	085859.83+050757.2	19.018	0.396	−0.357	−0.244	−0.142	13464 ± 97	7.48 ± 0.02	0.98
Cand 386	092001.94+005201.2	19.288	0.441	−0.373	−0.187	−0.141	13170 ± 145	7.78 ± 0.02	1.43
Cand 389	093955.29+054934.6	18.178	0.539	−0.344	−0.214	−0.278	12877 ± 90	7.68 ± 0.01	1.58
Cand 399	100354.41+063850.6	19.115	0.416	−0.336	−0.102	−0.239	14351 ± 62	7.81 ± 0.01	1.14
Cand 400	100618.54+605500.7	18.155	0.551	−0.283	−0.204	−0.105	14942 ± 55	7.70 ± 0.01	1.15
Cand 426	105353.89+520031.0	18.873	0.396	−0.358	−0.235	−0.429	15882 ± 41	6.40 ± 0.01	1.32
Cand 430	105850.47+432710.9	18.936	0.450	−0.372	−0.252	−0.097	13600 ± 43	7.35 ± 0.01	1.34
Cand 433	110200.07−004055.9	19.103	0.332	−0.364	−0.243	−0.149	14102 ± 127	7.94 ± 0.02	1.18
Cand 455	111908.64+033818.6	18.857	0.403	−0.338	−0.210	−0.212	13837 ± 113	7.81 ± 0.02	1.23
Cand 477	113807.13+143257.4	17.619	0.596	−0.283	−0.265	−0.220	12514 ± 76	7.24 ± 0.01	1.42
Cand 487	114344.96+052214.8	17.364	0.441	−0.358	−0.354	−0.178	14243 ± 55	7.73 ± 0.01	1.25

the continuum-corrected spectra, which help us resolve the $T_{\rm eff}$ and log g degeneracy problem, and the solutions are independent of the spectral resolution used. Our choice of spectral normalization (case 2 over case 1) does not change our results significantly (see Fig. 2). Table 1 presents our adopted values of $T_{\rm eff}$, log g, and χ^2. Figure 3 shows our best-fit model spectra (*solid lines*) to the observed spectra (*jagged lines*) of low-mass WD candidates identified by Brown et al. (2006).

Repeat observations of one of our targets over several nights shows that our real errors are larger than our internal error estimates (in Table 1). Analyzing nine different spectra of the same object, we find that the average internal errors in $T_{\rm eff}$ and log g are 40 K and 0.02 dex, respectively, while the empirical estimates indicate 600 K and 0.08 dex. The real error bars (set by systematic errors in our analysis) are more like 5% in $T_{\rm eff}$ and 0.08 dex in log g.

2.2. *Results*

A glance at our best-fit $T_{\rm eff}$ and log g-values given in Table 1 shows that the majority of the objects in our sample have log $g > 7$ and therefore, by our definition, are not ELM WDs. This is completely at odds with the SDSS photometry, and we come back to this point in § 3. More importantly, the case of Cand 171 (J0917+46) deserves particular attention.

The WD J0917+46 has $T_{\rm eff} = 11{,}288 \pm 72$ K and log $g = 5.48 \pm 0.03$. The extremely low log g is identical to the log g estimate of the previous lowest mass WD candidate, J2049+00 (Eisenstein et al. 2006). However, Eisenstein et al. find evidence of multiple minima, and the available photometry for J2049+00 is inconsistent with this solution (see § 3). In the case of our lowest gravity object, J0917+46, both the spectrum and the SED are consistent with the derived temperature and gravity. Figure 4 presents the χ^2 distribution of our fits to the J0917+46 spectrum, which shows no evidence of any other minima in the explored parameter space.

In order to demonstrate that our fit for J0917+46 is reliable, we present our fits to the flux-normalized line profiles in Figure 5. These fits follow Liebert et al. (2004), Kawka et al. (2006), and Bassa et al. (2006), who continuum correct their spectra of

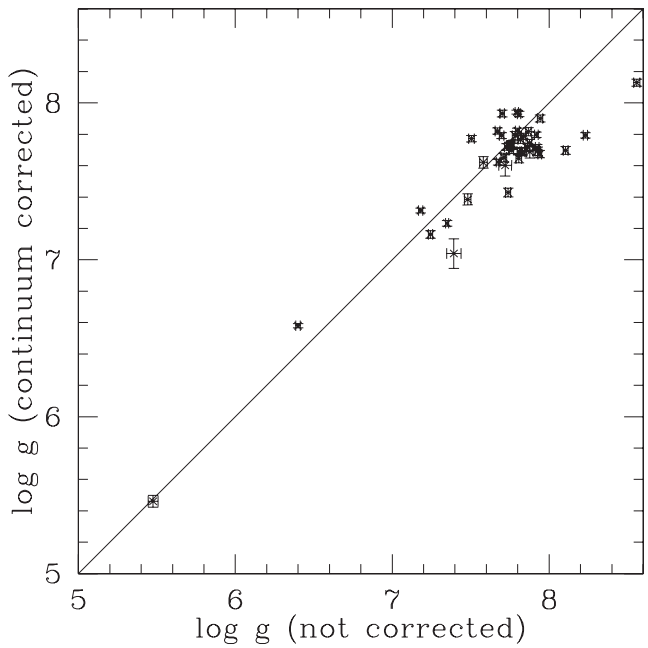

FIG. 2.—Plot of log g determinations using the line profiles from the continuum-corrected spectra vs. using the observed spectra without any continuum correction.

low-mass WDs and fit just the Balmer lines. We note that the χ^2 (per degree of freedom) is slightly higher in this case (2.08) compared to the χ^2 derived from fitting the entire spectrum (1.45). However, the best-fit solution, $T_{\rm eff} = 10{,}760 \pm 99$ K and $\log g = 5.46 \pm 0.04$, nicely agrees with our solution presented in Figure 3 and Table 1. Thus, J0917+46 is the lowest gravity WD currently known.

3. UNDERSTANDING THE SDSS LOW-MASS WHITE DWARF SAMPLE

The discrepancy between the SDSS photometry and our spectroscopic analysis initially puzzled us. Even though SDSS photometry of all of our candidates was consistent with their ELM WD classification, only J0917+46 and J1053+52 turned out to have $\log g < 7$. What went wrong? We begin by comparing the SEDs of our low-mass candidates with the SDSS broadband photometry. We then reanalyze the spectra of other low-mass WD candidates previously found in SDSS.

3.1. *Discrepant SDSS Photometry*

We have examined the SEDs of our candidates obtained from the SDSS photometry and compared them to our best-fit solutions from spectroscopy. We have applied the following AB

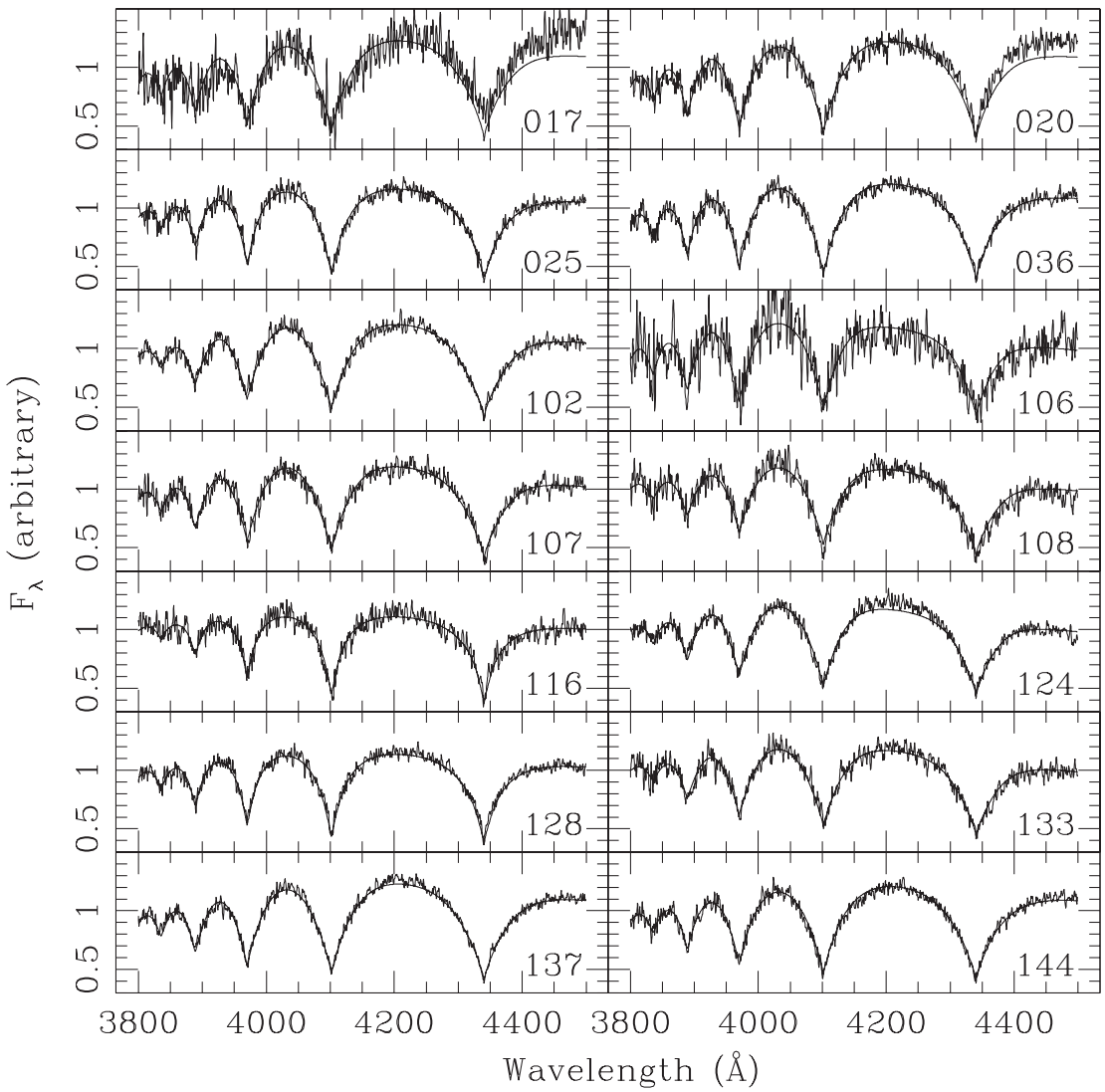

FIG. 3.—Spectral fits (*solid lines*) to the MMT spectra (*jagged lines*) of low-mass WD candidates. Candidate names are given in the lower right corner of each panel. [*See the electronic edition of the Journal for a color version of this figure.*]

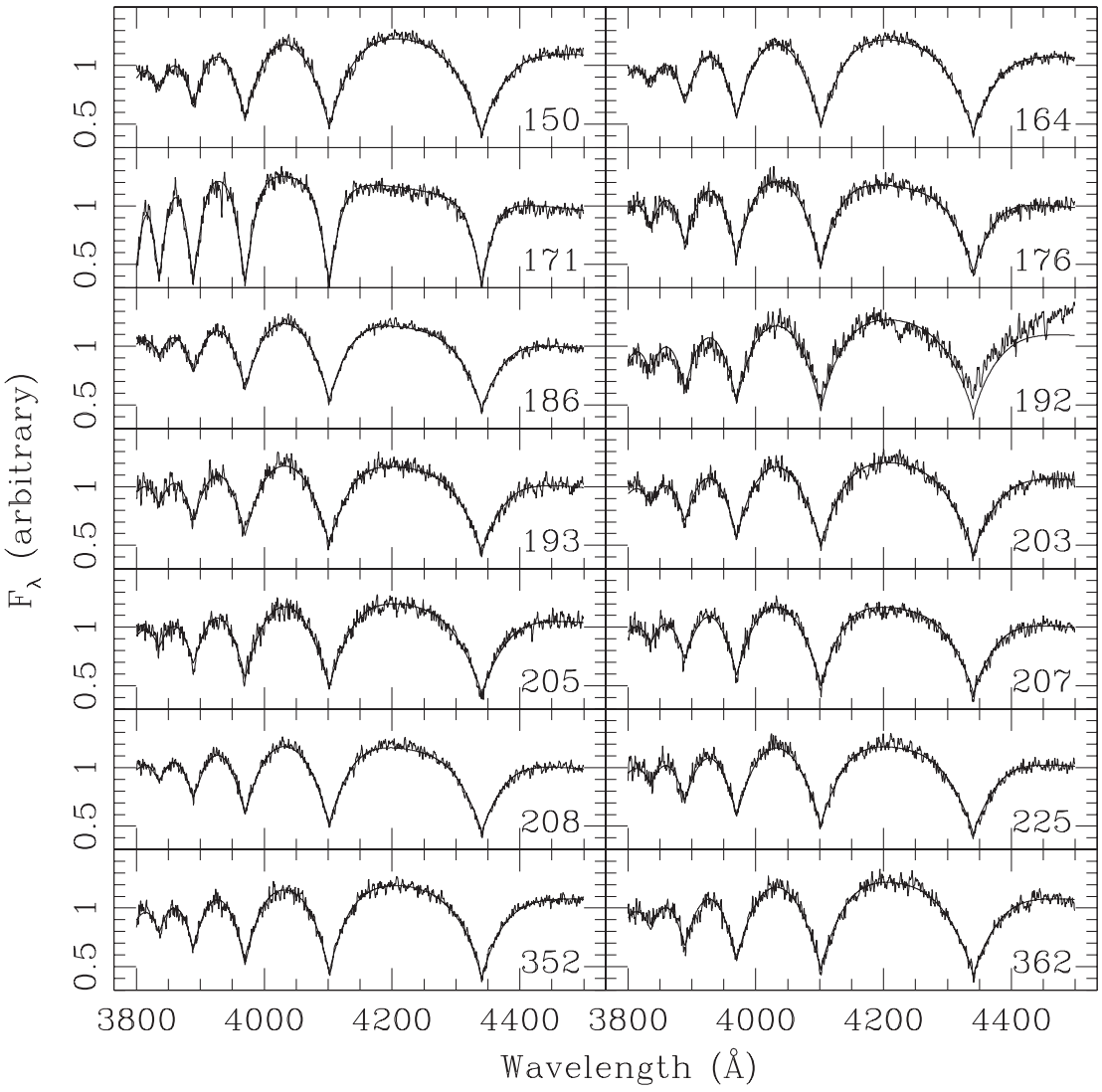

FIG. 3—*Continued*

corrections to the observed SDSS magnitudes: $u - 0.04$, $i + 0.015$, $z + 0.03$, and no corrections in g and r (see Eisenstein et al. 2006). The SDSS database gives the total interstellar absorption and reddening along the line of sight for each star, determined from the dust emission maps of Schlegel et al. (1998). Since all of our targets are at relatively high Galactic latitudes, the total absorption and reddening are small; the median total absorption A_g is 0.11, and the median total reddening $E(g-i)$ is 0.05. Therefore, the errors in the reddening corrections have little effect on our analysis.

We have calculated the predicted fluxes from our best-fit model atmosphere by integrating over the SDSS filter bandpasses. Without knowing the radii and distances to the WDs, we have used a χ^2 minimization technique to match the predicted fluxes with the observed fluxes. The value of χ^2 is taken as the sum over all bandpasses of the difference squared between the predicted and observed fluxes, properly weighted by the corresponding observational uncertainties.

Figure 6 shows the SEDs of four of the objects observed at the MMT plus the lowest mass WD candidate identified by Eisenstein et al. (2006). The dereddened SDSS photometry and the fluxes predicted for the parameters derived from our spectroscopic analysis are shown as error bars and circles, respectively. A comparison of the photometry and our best-fit solutions shows that the SDSS g-band photometry is systematically discrepant. For example, our best-fit solution for J0745+18 and J1529+33 (*top two panels*) reproduce u, r, i, and z photometry reasonably well. However, the SDSS g magnitudes are 20%–30% brighter than expected for these two objects (as well as many other candidates in the MMT sample). In order to check if the discrepancy is caused by our small reddening correction, we have also compared the predicted fluxes to the observed (not dereddened) SDSS photometry and found the same discrepancy in the g band. Brighter g-band magnitudes cause the objects to have more positive $u-g$ colors and more negative $g-r$ colors that are consistent with low-mass WDs. This suggests that SDSS photometry cannot be used by itself to identify ELM WDs.

We note that the g-band magnitude for the previous lowest mass WD candidate, J2049+00 (Eisenstein et al. 2006), may also be suspect. The bottom panel of Figure 6 shows that the SED of J2049+00 is discrepant with its g-band magnitude, and thus, we revisit its identification as an ELM WD.

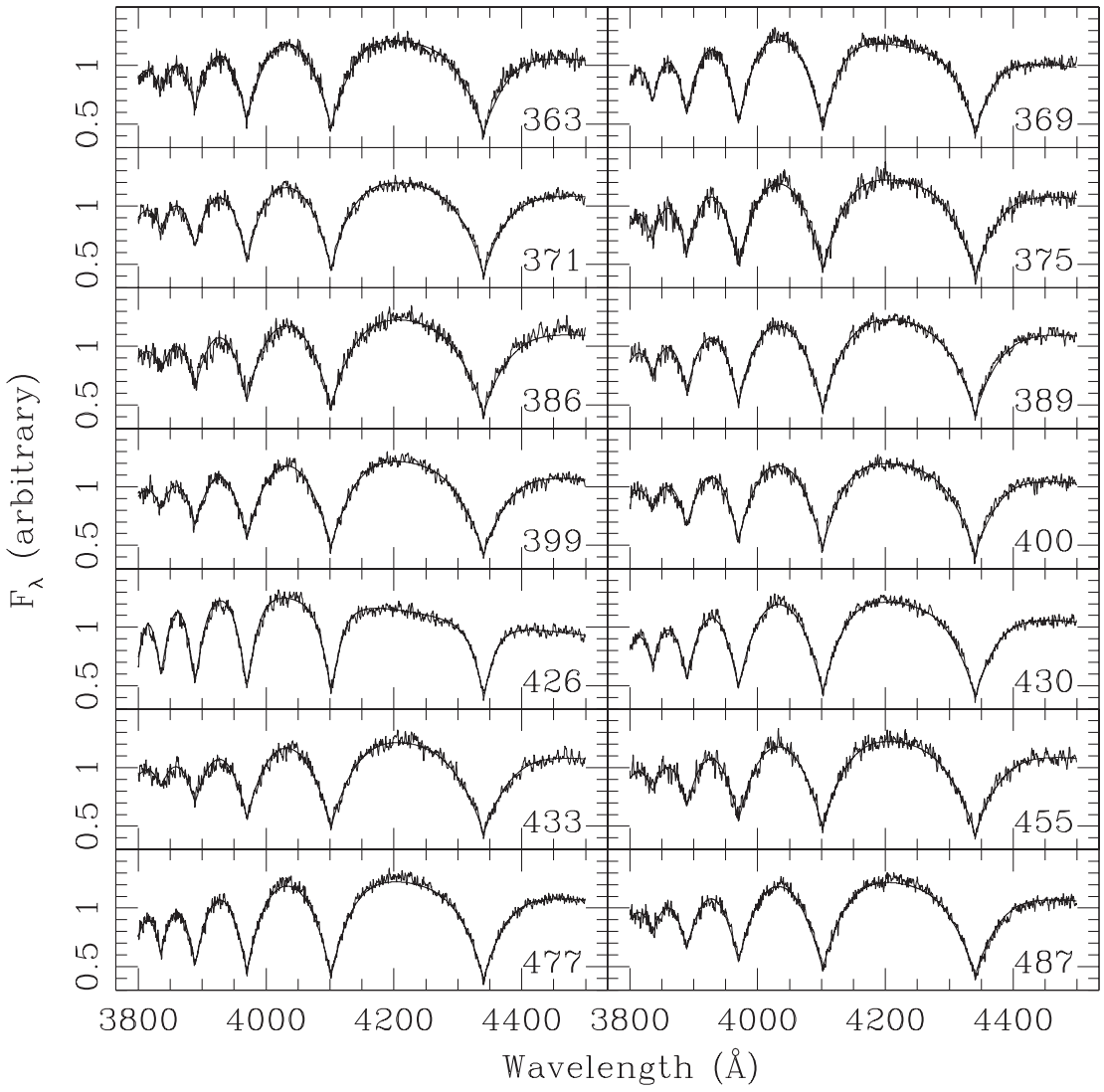

FIG. 3—*Continued*

3.2. *The SDSS Sample*

We now bring together the low-mass WD candidates previously found in SDSS. Kleinman et al. (2004) identified 2561 WDs, including several WDs with unusually low surface gravities, in the SDSS DR1 spectroscopy data. Liebert et al. (2004) performed model atmosphere analysis of two of these unusual WDs and found them to be ELM WDs. They have also found several other fainter low-mass WD candidates with noisy spectra. Eisenstein et al. (2006) study WDs across the entire SDSS DR4 and find 13 ELM WD candidates, including the ELM WD candidates identified in the SDSS DR1.

Eisenstein et al. (2006) use the same model atmospheres as we do; however, the log g sampling of their grid is coarser than ours (0.50 dex sampling compared to our 0.25 dex sampling). The procedure employed by Eisenstein et al. (see Kleinman et al. 2004) makes use of quadratic interpolation in χ^2 to find the location of the minimum with subpixel resolution, while our method performs quadratic interpolation in the model fluxes, which is more accurate. In addition to using the SDSS spectra from 3900 to 6800 Å, Eisenstein et al. also include SDSS colors in their fits. Using photometry can help constrain the temperature in the spectroscopic analysis of stars with reliable photometry. However, as we have demonstrated in § 2, it may not be ideal to analyze the outliers in color-color diagrams for which the SDSS photometry may be inaccurate. The lowest mass WD candidate found by Eisenstein et al. (2006) is an unfortunate example of this.

In order to confirm the ELM WD candidates found by Eisenstein et al. (2006), we use the same procedures for our MMT spectra to fit the SDSS sample. The SDSS spectra are noisier compared to our MMT data, and the derived parameters are therefore less reliable. We smooth the spectra to $R = 1000$ in order to increase the S/N, and the models are also degraded to the same resolution. We fit WD model atmospheres to the SDSS spectra in the spectral range 3800–4500 Å. The SDSS spectra are usually noisier in the red, and even including Hβ does not change our results significantly. Our temperature estimates differ significantly from the Eisenstein et al. (2006) estimates only for two WDs: J0822+27 and J1630+42. Using only spectroscopy led to best-fit solutions significantly different from the photometric estimates, and including the $g-r$ colors in our fits solved the problem for these two stars. The spectroscopic and photometric solutions agreed well for the rest of the SDSS sample. Figure 7 shows our best-fit models (*solid lines*) to the observed SDSS spectra (*jagged lines*) of low-mass WD candidates. Table 2 presents $T_{\rm eff}$ and log g

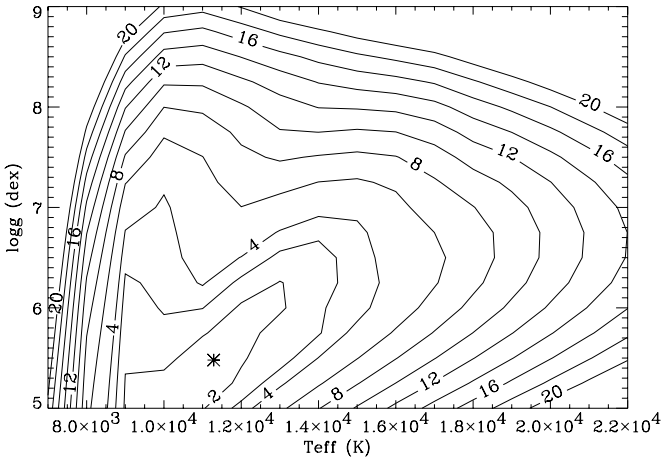

FIG. 4.—Contours of the χ^2 (per degree of freedom) distribution of our fits to the spectrum of the ELM WD J0917+46. An asterisk marks the location of the best-fit solution with a minimum $\chi^2 = 1.45$.

estimates from our study, and those from Liebert et al. (2004) and Eisenstein et al. (2006).

Comparisons of temperatures and surface gravities from our analysis, Liebert et al. (2004; *squares*), and Eisenstein et al. (2006; *circles*) are presented in Figure 8. Open symbols represent the objects with low S/N SDSS spectroscopy. This figure shows that our results for the two ELM WDs analyzed by Liebert et al. (2004) are consistent with their analysis. Our temperature estimates differ from Eisenstein et al. (2006) results by 141 ± 1520 K, and our surface gravity estimates are different by 0.13 ± 0.16 dex (excluding the two lowest gravity candidates). We note that one object, J1053+52, is common to both the MMT and SDSS samples. Our fits to the MMT spectrum of this object yield $T_{\rm eff} = 15{,}882 \pm 41$ K and $\log g = 6.40 \pm 0.01$, and the SDSS spectrum yields $T_{\rm eff} = 18{,}328 \pm 235$ K and $\log g = 6.40 \pm 0.05$. The nature of this object as an ELM WD is confirmed by our analysis.

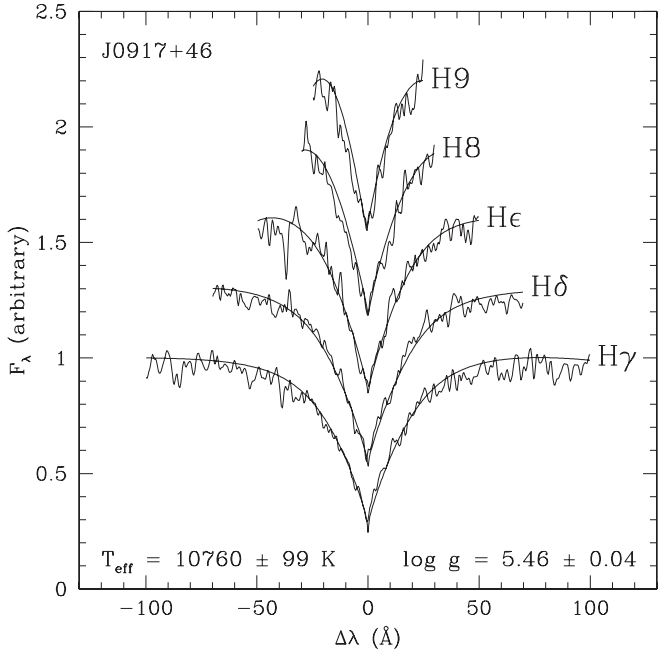

FIG. 5.—Spectral fits to the flux-normalized line profiles of J0917+46.

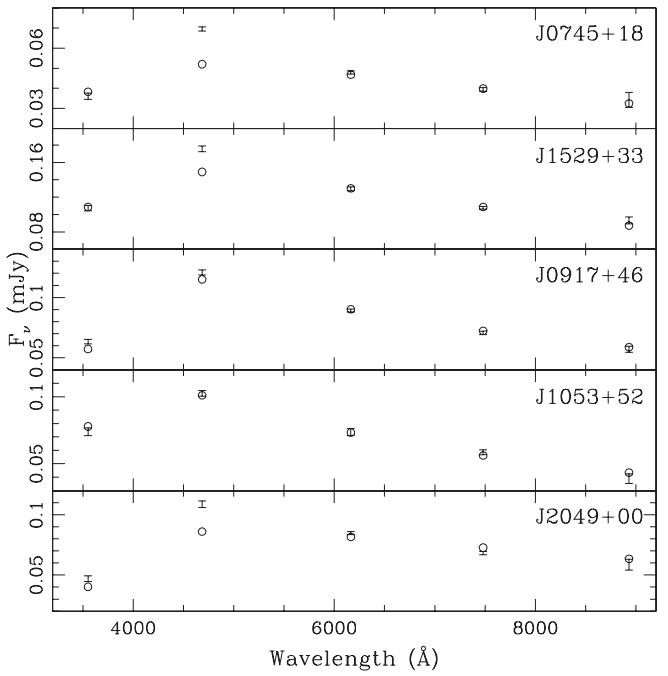

FIG. 6.—SEDs of four objects from our study and one object from Eisenstein et al. (2006). The SDSS photometry and the predicted fluxes from our best-fit solution to the spectra are shown as error bars and circles, respectively. The SDSS photometry and the best-fit solution for J2049+00 is taken from Eisenstein et al. (2006). J0745+18 and J1529+33 have $\log g > 8$, and they are good examples of objects with discrepant g-band photometry, which causes the colors for these objects to appear similar to low-mass WDs. J0917+46 and J1053+52 are true low-mass WDs with reliable SDSS photometry. The g-band photometry for J2049+00, the lowest mass WD candidate identified by Eisenstein et al. (2006), is also suspect, which suggests that it is not located in the $u-g$ vs. $g-r$ color-color region where we expect to find low-mass WDs.

One major difference between this work and Eisenstein et al. (2006) is that we find a best-fit solution of $\log g \leq 5$ for their lowest mass WD candidate, J2049+00. We have repeated our fits for this star by fitting the flux calibrated line profiles and also fitting the entire SDSS spectrum, and in both cases we find that the best-fit solution is exactly our lowest gravity model ($\log g = 5$). Eisenstein et al. (2006) find evidence for multiple minima in their fits for this star, and they conclude that the available photometry is more consistent with a lower gravity ($\log g < 5$) solution. Here we demonstrate that the SDSS spectrum of J2049+00 is also consistent with a lower gravity ($\log g < 5$) solution, and therefore, it is not a WD. We performed the Clewley et al. (2002) line shape test for the classification of halo A-type stars, but the results are ambiguous. The Hγ profile is marginally consistent with the star being a blue horizontal branch (BHB) star, but the Hδ profile is inconsistent with a BHB star. Based on H line indices we determine the spectral type of J2049+00 to be A2 with an uncertainty of ± 1.2 subtypes. If J2049+00 is an A star with $M_V \sim 1$, then it is located at $\sim$36 kpc. The lack of a significant proper motion in the USNO-B catalog is consistent with it being a distant A star.

Our fits also indicate that J0849+04 (with S/N < 10 spectroscopy), Eisenstein et al.'s (2006) second lowest mass WD candidate with $T_{\rm eff} = 9962$ K and $\log g = 5.93 \pm 0.15$, is better fit with a $T_{\rm eff} = 12{,}000 \pm 208$ K and $\log g = 7.34 \pm 0.07$ model atmosphere. Our fits to the Balmer lines (continuum-corrected spectrum) also result in a best-fit solution of $T_{\rm eff} = 12{,}397 \pm 91$ K and $\log g = 7.21 \pm 0.05$. Both of these fits suggest that J0849+04 is a low-mass WD, but not an ELM WD.

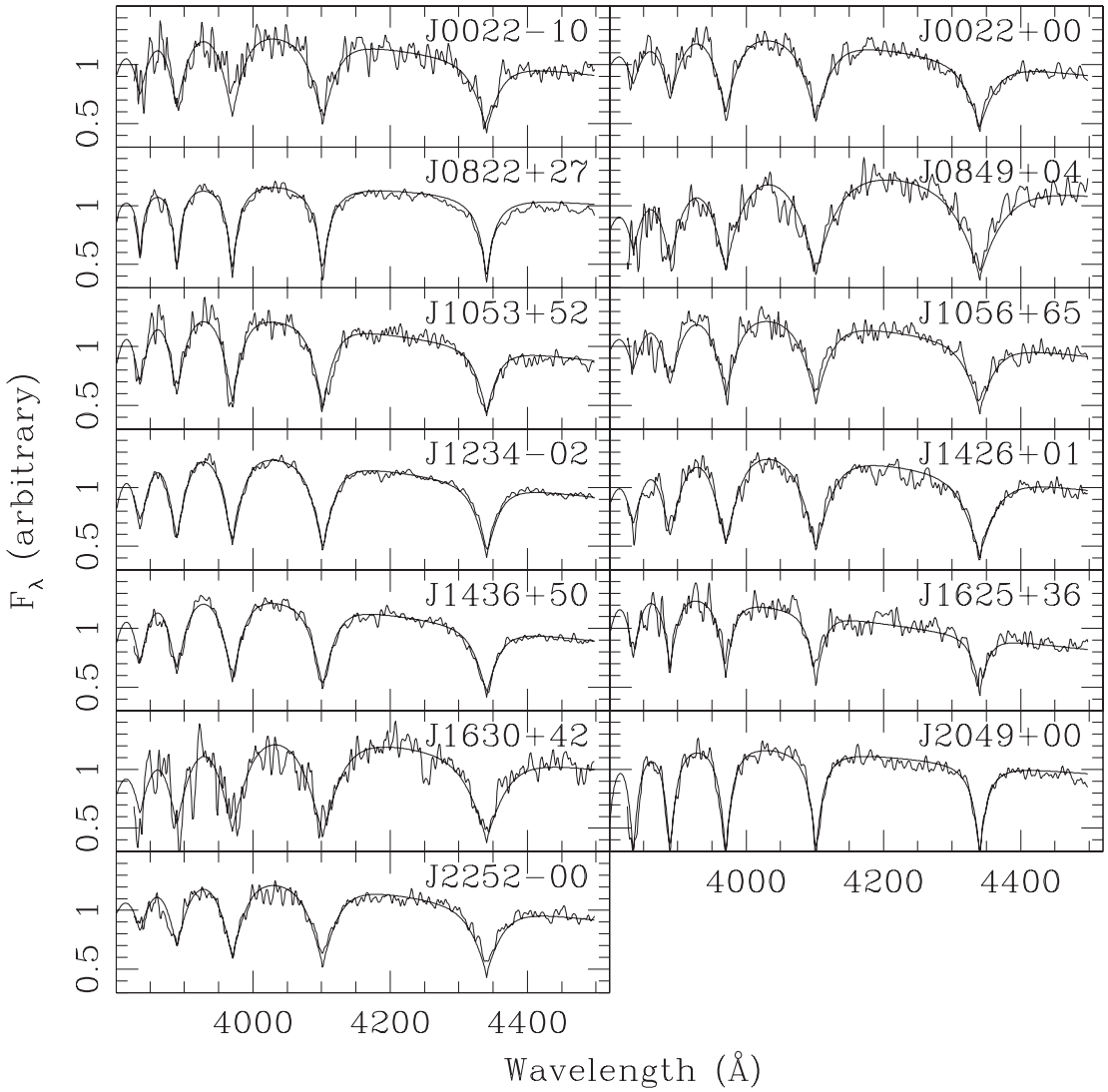

FIG. 7.—Spectral fits (*solid lines*) to the SDSS spectra (*jagged lines*) of low-mass WD candidates identified by Eisenstein et al. (2006). [*See the electronic edition of the Journal for a color version of this figure.*]

TABLE 2

LOW-MASS WHITE DWARF CANDIDATES IDENTIFIED BY EISENSTEIN ET AL. (2006)

Object	$T_{\rm eff}$ (K; this work)	log g (this work)	$T_{\rm eff}$ (K; SDSS)	log g (SDSS)	S/N[a]
J0022+00	19562 ± 153	7.12 ± 0.05	17355 ± 394	6.95 ± 0.11	9.6
J0022−10	18397 ± 299	6.82 ± 0.07	19444 ± 758	6.76 ± 0.16	7.0
J0822+27	8937 ± 48	7.21 ± 0.04	8777 ± 40	6.78 ± 0.11	20.3
J0849+04	12000 ± 208	7.34 ± 0.07	9962 ± 165	5.93 ± 0.15	8.5
J1053+52	18328 ± 235	6.40 ± 0.05	15399 ± 400	6.28 ± 0.11	10.7
J1056+65	19000 ± 151	7.03 ± 0.05	20112 ± 634	6.94 ± 0.12	9.4
J1056+65[b]			21910 ± 1900	7.07 ± 0.10	
J1234−02	16897 ± 78	6.49 ± 0.02	17114 ± 227	6.30 ± 0.05	21.2
J1234−02[b]			17470 ± 750	6.38 ± 0.05	
J1426+01	15869 ± 112	7.02 ± 0.03	16311 ± 359	6.92 ± 0.09	10.7
J1436+50	18339 ± 110	6.59 ± 0.02	16993 ± 229	6.58 ± 0.06	17.6
J1625+36	23000 ± 435	6.01 ± 0.07	24913 ± 936	6.20 ± 0.15	8.7
J1630+42	14183 ± 942	7.08 ± 0.07	14854 ± 359	6.89 ± 0.13	7.0
J2049+00	8581 ± 31	5.00 ± 0.12	8660 ± 144	5.48 ± 0.10	12.9
J2252−00	19114 ± 99	7.12 ± 0.03	20479 ± 433	6.85 ± 0.08	13.5

[a] S/N of the SDSS spectra in the g band.
[b] $T_{\rm eff}$ and log g fits by Liebert et al. (2004).

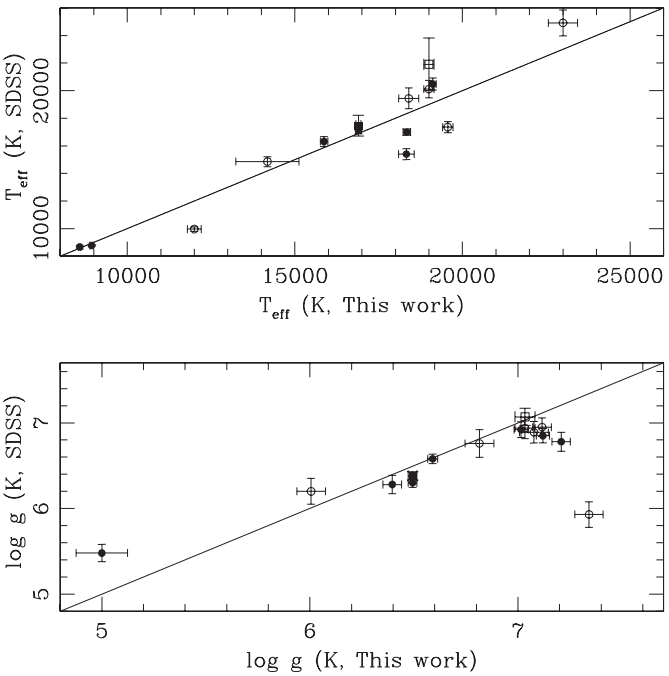

FIG. 8.—Eisenstein et al. (2006; *circles*) and Liebert et al. (2004; *squares*) fits to temperatures and gravities of ELM WD candidates found in the SDSS compared to our fits to the same stars. Objects with low S/N spectra (S/N $\leq$ 10 in the g band) are shown as open circles and squares. [*See the electronic edition of the Journal for a color version of this figure.*]

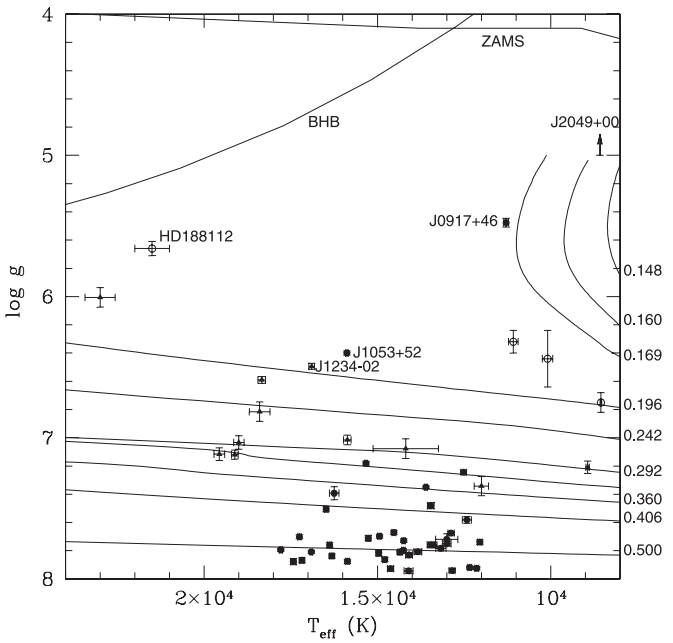

FIG. 9.—Our best-fit solutions for the surface gravity and temperatures of the low-mass WD candidates observed at the MMT (*filled circles*) and the SDSS (Eisenstein et al. 2006; *triangles*), overlaid on tracks of constant mass from Althaus et al. (2001). ZAMS and BHB star tracks are also shown. Spectroscopically confirmed ELM WDs found in the literature (HD 188112, LP 400−22, and companions to PSR J1012+5307 and PSR J1911−5958A) are shown as open circles. [*See the electronic edition of the Journal for a color version of this figure.*]

The rest of the objects in the Eisenstein et al. (2006) low-mass WD sample seem to have surface gravities in the range $\log g = 6$–7.3, and hence our analysis supports their classification as low-mass WDs. However, the SDSS spectroscopy for the majority of them is very noisy, especially in the blue, and a better understanding of these objects must await higher S/N spectroscopy.

4. DISCUSSION

Our spectroscopic analysis of the low-mass WD candidates in the SDSS shows that J0917+46 has $T_{\rm eff} = 11{,}288 \pm 72$ K and $\log g = 5.48 \pm 0.03$, and it is the lowest surface gravity WD currently known. We find one other ELM WD in our MMT sample, J1053+52. The remaining 40 candidates observed at the MMT are normal DA WDs with apparently inaccurate SDSS g magnitudes. We also confirm the low surface gravities of the ELM WD candidates identified by Eisenstein et al. (2006), with the exception of their lowest mass WD candidate.

Figure 9 shows the effective temperatures and surface gravities for the MMT (*filled circles*) and SDSS (*triangles*) samples plus the previously identified ELM WDs in the literature (*open circles*). Solid lines show the constant mass tracks for low-mass WDs[6] from Althaus et al. (2001; labeled in $M_\odot$ on the right side of the figure), and the tracks for zero-age main sequence (ZAMS) and horizontal branch stars. The zero-age BHB marks the location of the star at the start of the core-helium burning phase. Stars evolve upward to lower $\log g$-values as the He burning proceeds.

Figure 9 shows that the majority of the WDs found by Brown et al. (2006) have $M \sim 0.5\ M_\odot$. Only two objects, J0917+46 and J1053+52, have $M < 0.2\ M_\odot$. All of the low-mass WD candidates identified by Eisenstein et al. (2006), except J2049+00, have $M \leq 0.36\ M_\odot$; therefore, they should have formed in binary systems. None of the stars in the MMT sample or the SDSS sample show excesses in their SDSS photometry; therefore, the companions are likely to be compact objects. We have two separate spectra for J1053+52. We have measured a radial velocity of -53 ± 18 km s^{-1} from the MMT spectrum obtained on 2006 February 24, and a velocity of 11 ± 38 km s^{-1} from the SDSS observations obtained on 2003 January 10. The observed radial velocity change may be real; however, more accurate and time-resolved spectroscopic observations of this object, as well as all the other ELM WDs in our study, are required to constrain the mass of the unseen companion.

Figure 9 demonstrates that J0917+46 is an ELM WD and not a BHB or a main-sequence star. Its temperature and surface gravity imply an absolute magnitude of $M_V \sim 6.9$ (Althaus et al. 2001) and an age of 470 Myr. This luminosity places it at a distance of 2.6 kpc. At a Galactic latitude of $+44^\circ$, it is located at 1.8 kpc above the plane. J0917+46 has a proper-motion measurement of 0 mas yr^{-1} in the USNO-B catalog, which is consistent with a distant object. Our radial velocity measurement of 165 ± 12 km s^{-1} from the MMT spectroscopy corresponds to $U = -108$, $V = 25$, and $W = 122$ km s^{-1} (heliocentric), consistent with a thick disk or halo WD (Chiba & Beers 2000). If the observed radial velocity is due to the orbital motion of the star, then it would be more consistent with a thick disk WD.

Low-mass WDs can be produced in low-mass X-ray binaries (LMXBs; WD–neutron star binaries) or in a common-envelope

[6] The difference between the low-mass WD models below and above 0.18 $M_\odot$ is caused by element diffusion and thermonuclear flashes. WDs with $M > 0.18\ M_\odot$ suffer from several thermonuclear flashes, which consume most of the H-rich envelope. Element diffusion induces additional flashes, which ultimately leads to thinner H envelopes. As a result, when the final cooling branch is reached, these WDs will be characterized by a thin hydrogen envelope. The models with $M < 0.18\ M_\odot$ do not experience thermonuclear flashes even if diffusion is considered. As a result, they have massive hydrogen envelopes, and therefore, their radius will be considerably larger than the more massive counterparts (L. Althaus 2006, private communication).

phase with other companion stars. About 90% of the known LMXBs are located in the Galactic plane ($b \leq 20^{\circ}$; Ritter & Kolb 2003). If J0917+46 had a neutron star companion, we would need an explanation for its peculiar location above the Galactic plane. The unusually high velocity of another extremely low mass WD, LP 400-22 (Kawka et al. 2006), indicates that LP 400-22 may have been released from its close binary. A similar scenario may explain the peculiar location of J0917+46.

Althaus et al. (2001) models predict J0917+46 to have $M \sim 0.17\ M_{\odot}$, $L \sim 0.2\ L_{\odot}$, and $R \sim 0.12\ R_{\odot}$, about 9 times bigger than a typical $0.6\ M_{\odot}$ WD. Other calculations and mass radius relations should give similar results, within a few $0.01\ M_{\odot}$ (see Bassa et al. 2006). A close examination of the spectrum of this object reveals a Ca K line (Cand 171 in Fig. 3). The Ca K line has an equivalent width of 0.35 Å and a radial velocity measurement of 164 km s^{-1}; it is photospheric. The equivalent width of the Ca line is similar to the DAZs observed by Zuckerman et al. (2003) and Koester et al. (2005), and corresponds to an abundance of $\log(\mathrm{Ca/H}) = -5.89$ (nearly solar). J0917+46 has more Ca than many of the DAZs with circumstellar debris disks, and requires an external source for the observed metals (Kilic et al. 2006; Kilic & Redfield 2007). The star is located far above the Galactic plane where accretion from the interstellar medium is unlikely (Dupuis et al. 1993). The nature of the possible companion star needs to be determined before the Ca abundance can be explained.

Extremely low mass WDs seem to be rare. Eisenstein et al. (2006) found only 13 candidates in the SDSS DR4 area (4783 deg^2). We have identified two ELM WDs (one in common with their analysis) in 3000 deg^2. However, our search was limited to $-0.39 < g-r < -0.27$ (and therefore to $T_{\rm eff} > 11{,}000$ K for $\log g < 6$ WDs). Eisenstein et al. (2006) made an initial color cut to select their WD candidates for spectroscopic analysis. Their initial color cut included the $u-g$ versus $g-r$ region where we expect to find $\log g \geq 5$ WDs; however, they did not find any WD candidates with $M < 0.17\ M_{\odot}$.

Detailed calculations of the evolution of 1–3.5 $M_{\odot}$ stars in close binary systems with neutron stars show that the final mass of the He core WD produced in the process can be as low as $0.02\ M_{\odot}$ (Benvenuto & De Vito 2005). Ergma et al. (1998) argued that if the initial orbital period of a 1 $M_{\odot}$ Population II object in a binary system with a neutron star is less than 0.95 days, the orbital evolution of the system would proceed toward very short orbital periods, and these systems would end their evolution as ultracompact LMXBs with a WD secondary mass of $\leq 0.1\ M_{\odot}$ (e.g., 4U 1820−30 is an LMXB with an orbital period of 11 minutes and an estimated secondary mass of $M \sim 0.06$–$0.08\ M_{\odot}$; Stella et al. 1987; Rappaport et al. 1987). They also argued that if the initial orbital period of the system is between 0.95 and ∼1.50 days (the upper limit is the bifurcation orbital period), the systems would evolve toward shorter orbital periods and LMXBs with orbital periods of ≥10 hr will be formed. Ergma et al. (1998) found that the lowest mass WDs in such systems would be 0.15–0.16 and $0.17\ M_{\odot}$ for Population I and II stars, respectively. These low-mass limits also seem consistent with the analysis of Benvenuto & De Vito (2005).

Binary millisecond pulsar systems with low-mass WD secondaries are thought to be the descendants of the LMXBs. All of the currently known WDs in the field and around the millisecond pulsars have masses larger than $0.17\ M_{\odot}$. The masses of some of these WDs have been determined from the Shapiro (1964) delay of the pulsar signal in the gravitational field of the companion WD (Löhmer et al. 2005). This delay is linearly proportional to the mass of the companion, and therefore, the nondetection of $M < 0.17\ M_{\odot}$ WDs around pulsars may be an observational bias. A more targeted search for these objects may find WDs with smaller masses; however, identifying these low-gravity objects as low-mass WDs may be challenging. On the other hand, if the binary formation models of low-mass He core WDs around neutron stars are correct, we would expect to find lower mass WDs only in ultracompact LMXBs and their descendants.

5. CONCLUSIONS

We have performed spectroscopic analysis of the low-mass WD candidates found in the SDSS. We have shown that SDSS J0917+46 is the lowest mass WD currently known with $M \sim 0.17\ M_{\odot}$. In addition, there are three more WDs in the SDSS with masses smaller than $0.2\ M_{\odot}$. These WDs presumably have unseen companions. A radial velocity search for these unseen companions will be necessary to constrain their masses and the evolutionary scenarios for the formation of extremely low mass WDs. So far, both of the spectroscopically confirmed $\sim 0.2\ M_{\odot}$ WDs with known companions (PSR J1012+5307 and J1911−5958A) are in 14.5–20 hr orbits around neutron star companions (van Kerkwijk et al. 1996; Bassa et al. 2006). If J0917+46 is in a binary system with a neutron star, we expect a similar orbital period.

The search for radio pulsars around eight low-mass WDs by van Leeuwen et al. (2006) did not find any pulsar companions, and they concluded that the fraction of low-mass He core WDs with neutron star companions is less than $18\% \pm 5\%$. However, their sample included only one WD with $M \sim 0.2\ M_{\odot}$ (SDSS J1234−02). Liebert et al. (2004) argued that if the binary separation is appropriate, it is possible to create an extremely low mass WD in a WD-WD binary as well. Time-resolved radial velocity measurements will be necessary to differentiate between these two formation scenarios. Excluding the ultrashort period LMXBs, the models for the formation of low-mass helium WDs in millisecond pulsar binary systems predict the lowest mass WDs to have $M \sim 0.17\ M_{\odot}$. J0917+46 may be an example of the lowest mass WDs produced in such systems.

We would like to thank Marc Pinsonneault, Gregory Sivakoff, and Andrew Gould for helpful discussions. We also thank our anonymous referee for useful suggestions.

REFERENCES

Allende Prieto, C. 2004, Astron. Nachr., 325, 604
Althaus, L. G., Serenelli, A. M., & Benvenuto, O. G. 2001, MNRAS, 323, 471
Bassa, C. G., van Kerkwijk, M. H., Koester, D., & Verbunt, F. 2006, A&A, 456, 295
Benvenuto, O. G., & De Vito, M. A. 2005, MNRAS, 362, 891
Bergeron, P., Leggett, S. K., & Ruiz, M. T. 2001, ApJS, 133, 413
Brown, W. R., Geller, M. J., Kenyon, S. J., & Kurtz, M. J. 2006, ApJ, 647, 303
Chiba, M., & Beers, T. C. 2000, AJ, 119, 2843
Clewley, L., Warren, S. J., Hewett, P. C., Norris, J. E., Peterson, R. C., & Evans, N. W. 2002, MNRAS, 337, 87
Dupuis, J., Fontaine, G., & Wesemael, F. 1993, ApJS, 87, 345
Eisenstein, D. J., et al. 2006, ApJS, 167, 40
Ergma, E., Sarna, M. J., & Antipova, J. 1998, MNRAS, 300, 352
Finley, D. S., Koester, D., & Basri, G. 1997, ApJ, 488, 375
Gianninas, A., Dufour, P., & Bergeron, P. 2004, ApJ, 617, L57
Heber, U., Edelmann, H., Lisker, T., & Napiwotzki, R. 2003, A&A, 411, L477

Kawka, A., Vennes, S., Oswalt, T. D., Smith, J. A., & Silvestri, N. M. 2006, ApJ, 643, L123
Kilic, M., & Redfield, S. 2007, ApJ, 660, 641
Kilic, M., von Hippel, T., Leggett, S. K., & Winget, D. E. 2006, ApJ, 646, 474
Kleinman, S. J., et al. 2004, ApJ, 607, 426
Koester, D., Rollenhagen, K., Napiwotzki, R., Voss, B., Christlieb, N., Homeier, D., & Reimers, D. 2005, A&A, 432, 1025
Liebert, J., Bergeron, P., Eisenstein, D., Harris, H. C., Kleinman, S. J., Nitta, A., & Krzesinski, J. 2004, ApJ, 606, L147
Liebert, J., Bergeron, P., & Holberg, J. B. 2005, ApJS, 156, 47
Löhmer, O., Lewandowski, W., Wolszczan, A., & Wielebinski, R. 2005, ApJ, 621, 388
Marsh, T. R., Dhillon, V. S., & Duck, S. R. 1995, MNRAS, 275, 828
Massey, P., Strobel, K., Barnes, J. V., & Anderson, E. 1988, ApJ, 328, 315
Nelder, J., & Mead, R. 1965, Comput. J., 7, 308
Nice, D. J., Splaver, E. M., Stairs, I. H., Löhmer, O., Jessner, A., Kramer, M., & Cordes, J. M. 2005, ApJ, 634, 1242
Press, W. H., Flannery, B. P., Teukolsky, S. A., & Vetterling, W. T. 1986, Numerical Recipes: The Art of Scientific Computing (Cambridge: Cambridge Univ. Press)
Rappaport, S., Ma, C. P., Joss, P. C., & Nelson, L. A. 1987, ApJ, 322, 842
Ritter, H., & Kolb, U. 2003, A&A, 404, 301
Schlegel, D. J., Finkbeiner, D. P., & Davis, M. 1998, ApJ, 500, 525
Shapiro, I. I. 1964, Phys. Rev. Lett., 13, 789
Stella, L., Priedhorsky, W., & White, N. E. 1987, ApJ, 312, L17
van Kerkwijk, M. H., Bell, J. F., Kaspi, V. M., & Kulkarni, S. R. 2000, ApJ, 530, L37
van Kerkwijk, M. H., Bergeron, P., & Kulkarni, S. R. 1996, ApJ, 467, L89
van Leeuwen, J., Ferdman, R. D., Meyer, S., & Stairs, I. 2007, MNRAS, 374, 1437
Zuckerman, B., Koester, D., Reid, I. N., & Hünsch, M. 2003, ApJ, 596, 477